The dynamical implications of disease interference: Correlations and coexistence

Yunxin Huang[a,b,*], Pejman Rohani[a,b]

[a]*Institute of Ecology, University of Georgia, Athens, GA 30602, USA*
[b]*Biomedical and Health Sciences Institute, University of Georgia, Athens, GA 30602, USA*

Abstract

Ecological interference between unrelated diseases, caused by the temporary or permanent removal of individuals susceptible to one disease following infection with another, might be an important mechanism underlying epidemics. In this paper, we explore the potential dynamic consequences of interference by analyzing a two-disease model. By studying the stability domain of the model's equilibria, we find that the stable region of the two-disease endemic state becomes increasingly smaller as the strength of interference (largely determined by the disease-induced mortality) increases. When seasonal changes are included in the transmission rates, the bifurcation structure of the model's periodic cycles reveals that when the two diseases have similar mean transmission rates, multiple attractors in which the two diseases are strongly correlated can coexist, and that when the two diseases have very different mean transmission rates, the one with higher mean transmission rate may determine the dynamics of the system, with the other infection mimicking the behavior. We conclude that ecological interference can have important effects on the dynamical pattern of interacting diseases, the extent of which is determined by the epidemiological features of the diseases, their mean transmission rates in particular.

© 2005 Elsevier Inc. All rights reserved.

1. Introduction

Understanding the incidence and spread of infectious diseases has been a major focus of both empirical and theoretical epidemiologists (Anderson and May, 1991; Diekmann and Heesterbeek, 2000). The great microparasitic infections of childhood, such as measles and whooping cough, have received substantial attention from epidemiologists, due to the extensive available data sets documenting their spatio-temporal dynamics and the fascinating patterns observed in these data (e.g. Bartlett, 1956; Schenzle, 1984; Bolker and Grenfell, 1993, 1995; Rohani et al., 1999; Bauch and Earn, 2003).

Understanding the mechanisms underlying such epidemic behavior has been of great interest to mathematical epidemiologists, who have developed a suite of models, such as the well-known SIR and SEIR models, to study these issues (Dietz, 1976, 1979; Smith, 1983a, b; Aron and Schwartz, 1984; Kuznetsov and Piccardi, 1994; Earn et al., 2000).

Traditionally, epidemiologists have attempted to gain insight into the dynamics of a particular infection by focusing solely on the causative aetiological agent and the host, assuming no interaction with other pathogens. In recent years, single-host and single-pathogen approaches have been extended to incorporate multiple hosts and pathogens (Gupta et al., 1994; Gog and Swinton, 2002). These studies can be categorized according to the scale of interest: the antigenic or cellular scale and the population level. At the small

*Corresponding author. Institute of Ecology, University of Georgia, Athens, GA 30602, USA. Fax: +1 706 542 3580.

E-mail address: yxhuang@uga.edu (Y. Huang).

scale, studies have typically explored the immunological interaction between pathogens as a result of co-infection (Nowak and May, 1994; Kirschner, 1999). At the ecological level, shared pathogens have been demonstrated to be influential in shaping extinction dynamics by causing "apparent" competition between species (Tompkins et al., 2001). The issue that epidemics of unrelated pathogens might interact, however, has not been given the attention it deserves.

In 1979, Dietz proposed (as far as we are aware) the first one-host two-pathogen model to study the epidemics of adenoviruses. Since then, more complicated models have been developed, most of which have typically focused on the interactions between different strains of the same pathogen (Castillo-Chavez et al., 1989; Andreasen et al., 1997). Recently, Rohani et al. (1998, 2003) have proposed a mechanism underlying the interaction between antigenically distinct infections, such as measles and whooping cough. The mechanism that gives rise to an interaction is ecological (rather than immunological) and is based on the (temporary and/or permanent) removal of individuals from the susceptible pool for one pathogen following infection by a "competitor". A two-disease model has been developed to study this possible interaction. The results of this modeling work identified a negative correlation between the outbreaks of the two infections as the dominant signature of disease interference. Empirical patterns consistent with model predictions have been observed in historical European data (Rohani et al., 2003).

The previous work has focused exclusively on the scenario where interacting diseases have the same basic reproductive ratio. In this paper, we will explore the dynamical consequences of disease interaction further by studying a two-disease model. The following are the key questions we aim to answer:

(i) How does the (temporary or permanent) removal of individuals after infection with one disease affect the endemic equilibrium incidence of the other disease?

(ii) What are the range of dynamical attractors observed when the system is seasonally forced?

(iii) Is there a consistent relationship between the predicted dynamics of the two diseases?

(iv) How does the strength of interference depend on the two diseases' mean transmission rates?

(v) Under what circumstances will the epidemics of one disease mimic those of the other, exhibiting dynamics that cannot be found in a corresponding single-disease model?

In order to answer these questions, we will investigate the bifurcation structure of both the endemic states and the seasonally driven oscillations.

2. The two-disease SICR model

Consider two infectious diseases that compete for one host. Similar to Rohani et al. (1998), we assume the following simplified natural history of infection for each disease: individuals are *S*usceptible to infection at birth, upon contracting an infection an *I*nfectious period ensues, which is followed by *C*onvalescence upon clinical diagnosis. During the convalescence period, we assume that an individual is completely isolated from the rest of the population and that it could die as a result of infection. Upon *R*ecovery, the individual is considered permanently immune to the disease and is now only susceptible to the other disease if previously unexposed to it. A flow chart illustrating the epidemiologic process is given in Fig. 1. Note that for mathematical simplicity, we ignore the incubation period, but our qualitative results are not affected by this assumption. The important ingredients in the model that are predicted to give rise to interaction between different infections are (i) the convalescence period, and (ii) disease-induced mortality (DIM), which result in, respectively, temporary and permanent removal of individuals susceptible to one disease following infection with the other.
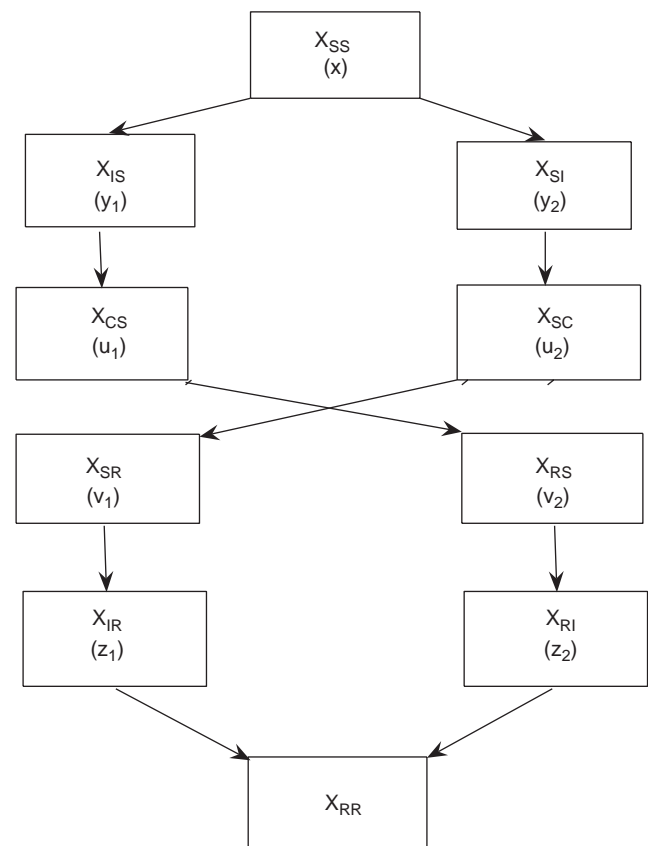

Fig. 1. A flow chart for the epidemiologic process in the two-disease model. The subscripts of the variable X indicate the infection history of individuals. Detailed explanation is given in the text.

The model is described as follows:

$$\dot{X}_{SS} = -\beta_1 X_{SS} X_{I.} - \beta_2 X_{SS} X_{.I} - \mu X_{SS} + \mu, \quad (2.1)$$

$$\dot{X}_{IS} = \beta_1 X_{SS} X_{I.} - (\gamma_1 + \mu) X_{IS}, \quad (2.2)$$

$$\dot{X}_{SI} = \beta_2 X_{SS} X_{.I} - (\gamma_2 + \mu) X_{SI}, \quad (2.3)$$

$$\dot{X}_{CS} = \gamma_1 X_{IS} - (\delta_1 + \rho_1 \delta_1 + \mu) X_{CS}, \quad (2.4)$$

$$\dot{X}_{SC} = \gamma_2 X_{SI} - (\delta_2 + \rho_2 \delta_2 + \mu) X_{SC}, \quad (2.5)$$

$$\dot{X}_{RS} = \delta_1 X_{CS} - \beta_2 X_{RS} X_{.I} - \mu X_{RS}, \quad (2.6)$$

$$\dot{X}_{SR} = \delta_2 X_{SC} - \beta_1 X_{SR} X_{I.} - \mu X_{SR}, \quad (2.7)$$

$$\dot{X}_{IR} = \beta_1 X_{SR} X_{I.} - (\gamma_1 + \mu) X_{IR}, \quad (2.8)$$

$$\dot{X}_{RI} = \beta_2 X_{RS} X_{.I} - (\gamma_2 + \mu) X_{RI}, \quad (2.9)$$

$$\dot{X}_{RR} = \gamma_1 X_{IR} + \gamma_2 X_{RI} - \mu X_{RR}. \quad (2.10)$$

Here $X_{I.} = X_{IS} + X_{IR}$ and $X_{.I} = X_{SI} + X_{RI}$ are the proportion of infectives with diseases 1 and 2, respectively. The subscripts for each variable reflect the infection history of individuals in that class. For example, X_{IS} represents the fraction of the total population who are infected with disease 1, and have not previously contracted disease 2. Note that no co-infection is assumed in the model. In addition, there are two more assumptions behind the model formulation. First, the total population has reached its demographic equilibrium which has been scaled to 1 in the absence of diseases, so the birth rate always matches the death rate (μ). Second, the population can increase its birth rate in response to disease-related deaths, which appears to be realistic for human population, so the total population still can approach to an equilibrium which would be slightly smaller than 1 if the birth rate remains to be μ. These two assumptions allow for a uniform model formulation for both cases (with and without disease-related deaths) after being scaled by the equilibrium population size. The description of model parameters are summarized in Table 1. While the notation concerning model variables is informative, it is also cumbersome. For this reason, we make the following substitutions: $x \equiv X_{SS}, y_1 \equiv X_{IS}, \ y_2 \equiv X_{SI}, \ z_1 \equiv X_{IR}, \ z_2 \equiv X_{RI}, \ u_1 \equiv X_{CS}, \ u_2 \equiv X_{SC}, \ v_1 \equiv X_{SR}, \ v_2 \equiv X_{RS}.$ The model with this notation, after dropping the equation for X_{RR} which is superfluous, becomes

$$\dot{x} = -\beta_1(y_1 + z_1)x - \beta_2(y_2 + z_2)x - \mu x + \mu, \quad (2.11)$$

$$\dot{y}_1 = \beta_1(y_1 + z_1)x - (\gamma_1 + \mu)y_1, \quad (2.12)$$

$$\dot{y}_2 = \beta_2(y_2 + z_2)x - (\gamma_2 + \mu)y_2, \quad (2.13)$$

$$\dot{u}_1 = \gamma_1 y_1 - (\delta_1 + \rho_1 \delta_1 + \mu)u_1, \quad (2.14)$$

$$\dot{u}_2 = \gamma_2 y_2 - (\delta_2 + \rho_2 \delta_2 + \mu)u_2, \quad (2.15)$$

$$\dot{v}_1 = \delta_2 u_2 - \beta_1(y_1 + z_1)v_1 - \mu v_1, \quad (2.16)$$

$$\dot{v}_2 = \delta_1 u_1 - \beta_2(y_2 + z_2)v_2 - \mu v_2, \quad (2.17)$$

$$\dot{z}_1 = \beta_1(y_1 + z_1)v_1 - (\gamma_1 + \mu)z_1, \quad (2.18)$$

$$\dot{z}_2 = \beta_2(y_2 + z_2)v_2 - (\gamma_2 + \mu)z_2. \quad (2.19)$$

In order to make latter expressions more compact and informative, we introduce a few groups of parameters

$$R_i \equiv \frac{\beta_i}{\gamma_i + \mu}, \quad i = 1, 2, \quad (2.20)$$

$$q_i \equiv \frac{\gamma_i}{\delta_i(1 + \rho_i) + \mu}, \quad i = 1, 2 \quad (2.21)$$

and

$$a_i \equiv \frac{\delta_i}{\delta_i(1 + \rho_i) + \mu} \cdot \frac{\gamma_i}{\gamma_i + \mu}, \quad i = 1, 2, \quad (2.22)$$

where the first group is known as *the basic reproductive ratios*.

3. Constant transmission rates: Equilibria and their bifurcations

For two-disease interactions, one of the fundamental questions is under what conditions is coexistence possible. The question can be studied straightforwardly by examining the existence and stability of model equilibria. When the transmission rates of both diseases (β_1 and β_2) are constant, there are up to 4 equilibria, depending on parameter values: the disease-free equilibrium E_1; the single-disease endemic equilibria E_2 and E_3; and the two-disease endemic equilibrium E_4. It is not difficult to derive the condition for the existence of all equilibria and the stability of E_1, E_2, E_3 by following the computational procedure outlined by Dietz (1979) (see Appendix A). An analytical proof for the stability of E_4 and the exclusion of Hopf bifurcation are, however, far from straightforward. Gumel et al. (2003) have numerically derived a normal form with a Lotka–Volterra type of competitive interaction at the neighborhood of the co-dimension-2 point $(R_1, R_2) = (1, 1)$ (for a two-disease "SEICR" model) (Kuznetsov, 1998) and demonstrated that the two-disease endemic equilibrium must be stable when both single-disease equilibria lose their stability and that there is no Hopf bifurcation associated with the two-disease endemic equilibrium. We found, by intensive numerical experiments with AUTO (Doedel et al., 1998), that these results are also true for our two-disease "SICR" model under the parameter setting considered. However, we do not exclude the possibility of Hopf bifurcations associated with equilibrium E_4 for other parameter settings that we have not explored in this paper. Combining with the bifurcation conditions which can be calculated analytically, we may summarize the results for the equilibria of our model as follows:

(i) when $R_1 < 1$ and $R_2 < 1$ there is only a stable disease-free equilibrium, E_1.

(ii) when $R_1 > 1$ and

$$\frac{R_1}{1 + a_1(R_1 - 1)} > R_2 \quad (3.1)$$

Table 1
Brief description of parameters

	Parameter description
μ	Per-capita natural death rate
β_i	Transmission probability per unit time per contact associated with disease i
$1/\gamma_i$	Average infectious period for disease i (prior to being quarantined)
$1/\delta_i$	Average convalescent or quarantined period for disease i
ρ_i	Disease-induced mortality which may be expressed as $-\ln(1-p)$ in which $p \in [0,1)$ is the disease-induced probability of dying

only disease 1 persists, giving rise to a unique stable equilibrium E_2.

(iii) when $R_2 > 1$ and

$$\frac{R_2}{1 + a_2(R_2 - 1)} > R_1 \qquad (3.2)$$

only disease 2 persists, giving rise to a unique stable equilibrium E_3.

(iv) otherwise, there is a stable coexistent equilibrium E_4.

These results can be further illustrated by way of a bifurcation diagram (see Fig. 2) which allows us to explore how disease-induced mortality (i.e. ρ_i, which will be abbreviated as *DIM* hereafter,) affects the likelihood of stable coexistence. By contrasting the stable coexistence regions for different DIMs, we find that the domain of coexistence shrinks when the DIM of one or both diseases increases (the region bounded by the two solid-line curve shrinks to the region bounded by the two dashed-line curves). More precisely, the higher the DIM of one disease, the harder it is for the other disease to invade.

Having established the effect of the convalescent period and DIM on coexistence, we explore their effects on disease incidence. To this end, we plot (in Fig. 3) the equilibrium level of incidence of disease 1 ($y_1^* + z_1^*$) as the convalescent period ($1/\delta_2$) and the DIM of disease 2 (ρ_2) vary. We find that at the equilibrium level, the incidence of one disease is negatively related to the DIM of the other disease, which is not surprising because the death caused by one disease reduces the number of susceptible individuals to the other. So, it is the DIM rather than the convalescent period that plays the key role.

One may further ask how much is the fraction of population that are not available for one disease due to the presence of the other disease. To see that, we plot, for different basic reproductive ratios, the percent of the population at equilibrium that are not available for disease 2 against the convalescent period for disease 1
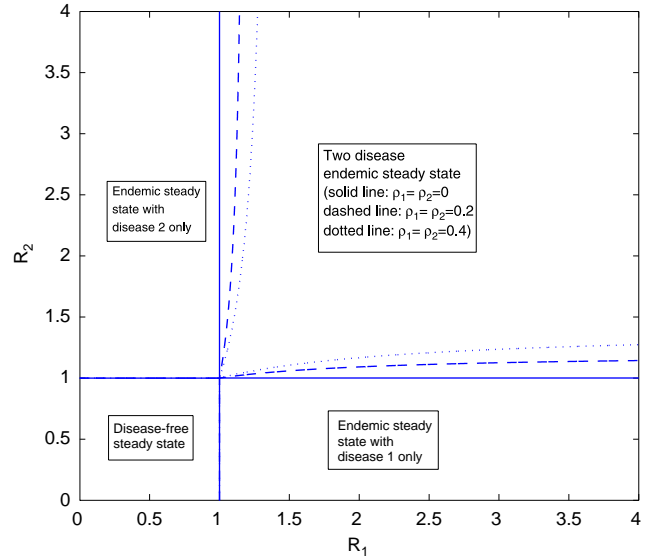

Fig. 2. A two parameter bifurcation diagram for the two-disease SICR model. In this diagram, we contrast the case where the disease-induced mortality is ignored ($\rho_1 = \rho_2 = 0$) with the cases where it is incorporated (for $\rho_1 = \rho_2 = 0.2$ and $\rho_1 = \rho_2 = 0.4$). For each pair of ρ_1 and ρ_2, the (R_1, R_2) parameter space is divided into 4 regions by 4 bifurcation curves. The other parameters are as follows: $\mu = 0.02$, $\gamma_1 = \gamma_2 = 45$, $\delta_1 = \delta_2 = 50$. Namely, the average life expectancy of the host is 50 years, the infectious periods are identically 0.01 year, and the convalescent periods are identically 0.02 year.
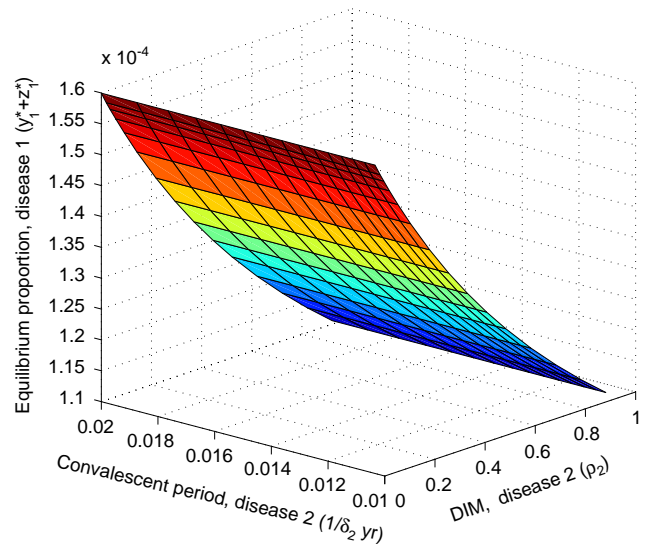

Fig. 3. A bifurcation diagram illustrating the equilibrium level of incidence of one disease in relation to the two interference parameters determined by the other disease. It is seen that at the equilibrium level, the incidence level of one disease is negatively related to the DIM of the other disease. The values of the other fixed parameters are the same as in Fig. 2.

(Fig. 4). As shown in the figure, the presence of disease 1 reduces the population available for disease 2 in a scale of one percent. Thus, the presence of one disease does
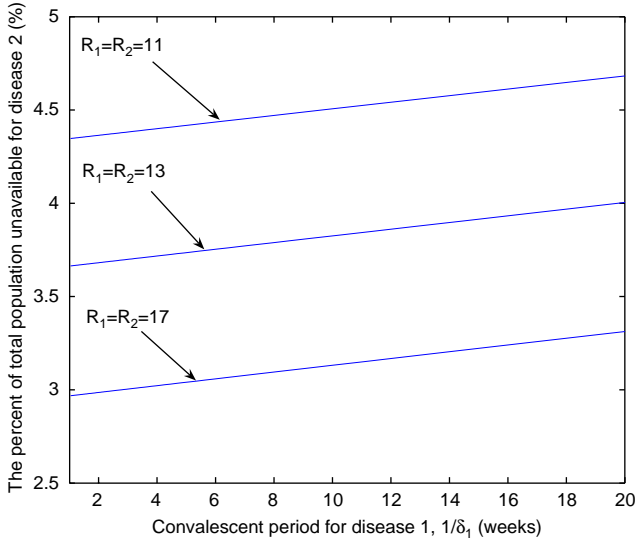
Fig. 4. A one-parameter bifurcation diagram in the two-disease model in which the effect of one disease on the other disease (at equilibrium) is quantified. Fixed parameters: $\gamma_1 = \gamma = 45$, $\delta_2 = 50$, $\rho_1 = \rho_2 = 0$, $\mu = 0.02$.

not seem to affect the magnitude of the population associated with the other disease greatly.

4. Seasonally forced transmission rates: Periodic cycles and their bifurcations

Now we consider the case where the transmission rates are seasonally varying, which is intended to mimic the transmission consequences of aggregation of children in schools. More precisely, we assume that the transmission rates change according to the following functional form:

$$\beta_i(t) = \beta_{i0}(1 + \sigma \cos 2\pi t), \quad i = 1, 2. \tag{4.1}$$

Here β_{i0} is the mean transmission rate of disease i and σ measures the seasonal amplitude. The time is scaled to units of year, so the period of seasonality is 1 year.

When one or both transmission rates are seasonally forced, the two diseases will oscillate periodically. To demonstrate this and to explore possible bifurcation events we use continuation methods in AUTO (Doedel et al., 1998) as the principal numerical tool. The numerical procedure is the following:

- *Step* 1: Select a set of symmetric (identical for the two diseases) parameters that allow for a unique stable equilibrium E_4 (in the absence of seasonality ($\sigma = 0$)). The elements of this equilibrium can be computed

explicitly as follows:

$$x^* = \frac{\mu}{2w^* + \mu},$$

$$y_1^* = y_2^* \equiv y^* = \frac{Rw^*x^*}{\beta},$$

$$z_1^* = z_2^* \equiv z^* = \frac{w^*}{\beta} - y^*,$$

$$u_1^* = u_2^* \equiv u^* = \frac{\gamma}{\delta(1 + \rho) + \mu}y^*,$$

$$v_1^* = v_2^* \equiv v^* = \frac{\delta}{w^* + \mu}u^*,$$

where

$$w^* = \frac{\mu}{4}\{[(1 + a)R - 3]$$
$$+ \sqrt{(1 + a)^2 R^2 - 2R(3a - 1) + 1}\}$$

while $\beta, \gamma, \delta, \rho, R$ and a are the corresponding symmetric parameters.

- *Step* 2: Starting from this analytically known equilibrium, use AUTO to compute a branch of periodic solutions as the amplitude of seasonality in transmission rates (σ in (4.1)) is varied.
- *Step* 3: Track further bifurcations of the cycles for the amplitude of seasonality or any other parameters of interest.

4.1. "Similar" mean transmission rates: Complex interference patterns

As is pointed out in the introduction, it is important to examine how the dynamical patterns of interference are related to the competitive potentials of the two diseases, as characterized by their mean transmission rates (β_{i0}). To this end, we need to check how cycles (for a specific amplitude of seasonality) bifurcate as the difference between the mean transmission rates of the two diseases varies. As is summarized in Fig. 5, we have identified 4 bifurcation curves which divide the (σ, β_{10}) parameter space into 6 regions. The bifurcation scenario (for fixed β_{10}) can be briefly described as follows. For small σ, there are only stable annual cycles, as also found by Rohani et al. (1998). As σ increases, two period-doubling bifurcations ("PD1" and "PD2") occur, giving rise to, respectively, a type 1 biennial cycle in which the two diseases are negatively correlated and a type 2 biennial cycle in which the two diseases are positively correlated. When the type 1 biennial cycle (arising from "PD1") is continued (by changing σ), a fold bifurcation happens. The locus of this bifurcation in the (σ, β_{10}) parameter space is a curve labeled by "F1". When the type 2 biennial cycle (arising from "PD2") is continued (by changing σ), a fold bifurcation is also detected. The locus of this bifurcation in the
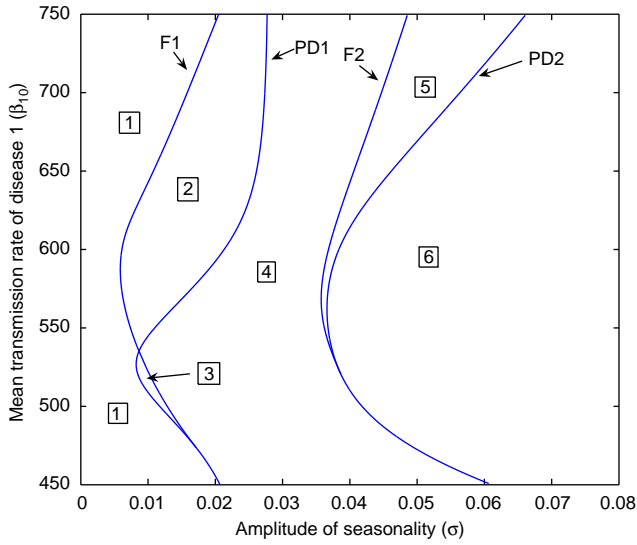
Fig. 5. A two parameter bifurcation diagram for the two-disease model with seasonal force in transmission rates. The two curves labeled by "PD1" and "PD2" are, respectively, the loci of two-period-doubling bifurcations of an annual cycle, while the two curves labeled by "F1" and "F2" are, respectively, the loci of two fold bifurcations of the biennial cycles arising from, respectively, "PD1" and "PD2". The meaning and the existence and stability of the cycles are described in the main text and summarized in Table 2. Fixed parameters: $\beta_{20} = 600$, $\gamma_1 = \gamma_2 = 45$, $\delta_1 = \delta_2 = 50$ and $\rho_1 = \rho_2 = 0$.

(σ, β_{10}) parameter space, labeled by "F1", lies to the left of "PD2". When the type 2 biennial cycle is continued further, a period-doubling bifurcation can be found (which is not shown in the diagram so as to focus on the bifurcation events for small amplitude of seasonality), giving rise to 4-year cycles. In the (δ, β_{10}) parameter space the existence and stability of cycles in various regions, as confirmed numerically, can be described as follows:

- In region 1 there is only a stable annual cycle.
- In region 2, a stable annual cycle and a type 1 biennial cycle (and an unstable biennial cycle) coexist.
- In region 3, there is a stable type 1 biennial cycle (together with an unstable annual cycle and an unstable biennial cycle).
- In region 4, there are a stable type 1 biennial cycle and an unstable annual cycle.
- In region 5, there are a stable type 1 biennial cycle, an unstable type 2 biennial cycle and an unstable annual cycle).
- In region 6, a stable type 1 biennial cycle and a stable type 2 biennial cycle coexist. There is also an unstable annual cycle.

The meaning and the existence and stability of the cycles are summarized in Table 2. The three types of cycle are given in Fig. 6.

Table 2
Existence and stability of the relevant cycles

	Annual	Biennial⁻	Biennial⁺
Region 1	s	n	n
Region 2	s	s	n
Region 3	u	s	n
Region 4	u	s	n
Region 5	u	s	u
Region 6	u	s	s

Biennial⁻ and Biennial⁺ represent, respectively, the negatively and positively correlated biennial cycles. The symbols "*n*", "*s*" and "*u*" mean, respectively, non-existent, stable and unstable.
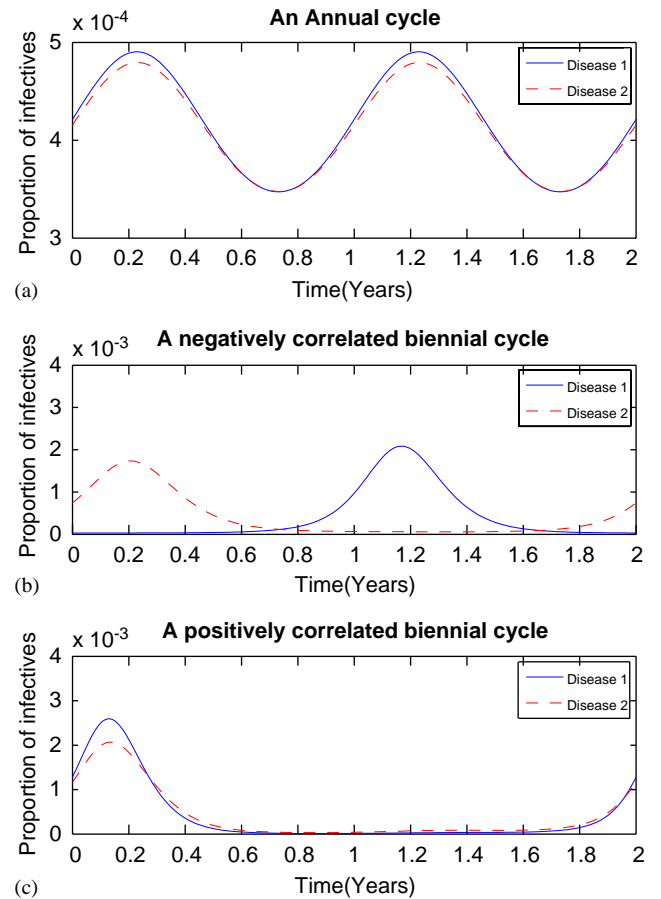

Fig. 6. Typical stable cycles as found in the various regions of Fig. 5. (a) an annual cycle ($\beta_{10} = 700$, $\sigma = 0.0125$, in region 1), (b) a negatively correlated biennial cycle ($\beta_{10} = 673$, $\sigma = 0.0345$, in region 4) and (c) a positively correlated biennial cycle ($\beta_{10} = 649$, $\sigma = 0.0797$, in region 6).

Next, we compute and plot the locus of the period-doubling point "PD2" in (β_{10}, β_{20}) parameter space for a fixed amplitude of seasonality in region 6. It turns out that the locus is a loop (see Fig. 7). Inside the loop, where the mean transmission rates of the two diseases are "similar", the two types of stable biennial cycles, in which the two disease strongly correlated, can coexist,
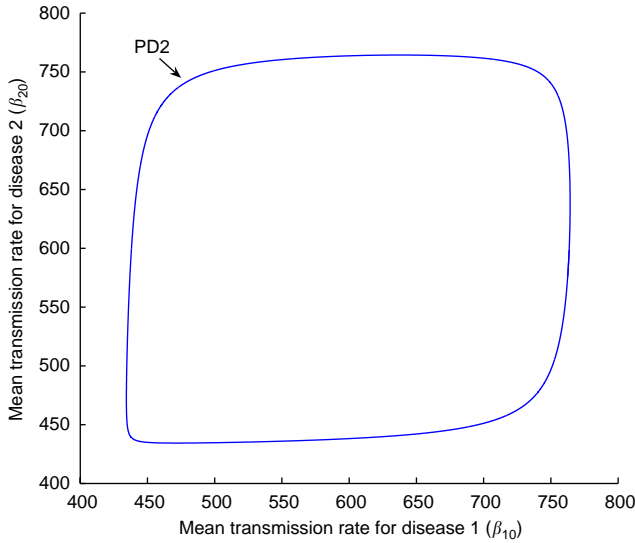
Fig. 7. A two-parameter bifurcation diagram for the two-disease model. Inside the loop, where the two diseases have "similar" basic reproductive ratios (or more precisely, mean transmission rates), the two types of stable biennial cycles (i.e. the positively and negatively correlated biennial cycles) can coexist, in contrast to the situation outside the loop, where dynamical patterns are relatively simple. Note that the amplitude of seasonality is fixed ($\sigma = 0.0687$). The other fixed parameters: $\gamma_1 = \gamma_2 = 45$, $\delta_1 = \delta_2 = 50$ and $\rho_1 = \rho_2 = 0$.
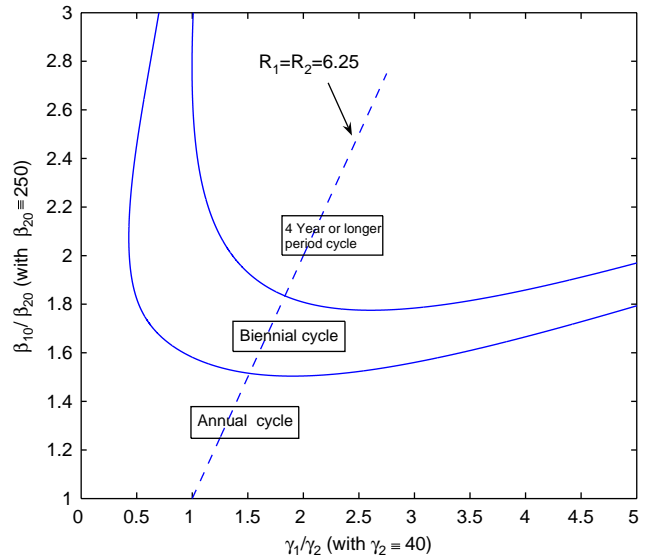

Fig. 8. A two-parameter bifurcation diagram for the two-disease model. When the mean transmission rate of disease 1 (β_{10}) is not very large, the model has only annual cycles. When β_{10} becomes increasingly larger, biennial cycles as well as other longer period cycles arise. The figure shows that one disease with a relatively high mean transmission rate (and an appropriate infectious period) can dominate the dynamics of the system, with the other infection mimicking the behavior. $\sigma = 0.111$. $\delta_1 = \delta_2 = 35$, $\rho_1 = \rho_2 = 0$.

in contrast to the situation outside the loop, where dynamical patterns are relatively simple, with only negatively correlated stable biennial cycles being possible.

4.2. "Dissimilar" mean transmission rates: One disease mimics the other

It has been demonstrated (both here and in Rohani et al., 1998, 2003) that it is possible for a disease, such as whooping cough, which exhibits rigidly annual cycles in single-disease models, to exhibit biennial cycles in two-disease models. In this subsection, we explore possible mechanisms underlying this observation. To address this question, we employ the following numerical procedure. First, we choose a set of symmetric (i.e. identical for both diseases) parameters for which the two-disease model has only annual cycles. Second, we fix an appropriate strength of seasonal force (σ) to look for possible bifurcations of the annual cycle from which biennial cycles may arise, as the transmission rate of disease 1 (β_{10}) varies. Third, we compute the locus of such a bifurcation point in the (β_{10}, γ_1) parameter space once it is detected. As is presented in Fig. 8, we have indeed found a period-doubling bifurcation of the annual cycle from which a biennial cycle, in which both diseases oscillate out of phase, arises. Note that the characteristic parameters associated with disease 2 (β_{20} and γ_2) always remain constant. Therefore, it is disease 1

(with a relatively high mean transmission rate and an appropriate infectious period) that induces disease 2 to mimic the behavior, exhibiting biennial oscillations that are not possible in the corresponding single-disease model. A typical biennial cycle of disease 2 is shown in Fig. 9. It should be pointed out, as seen in Fig. 8, that the period-doubling bifurcations occur even when the two diseases have equal basic reproductive ratios. This suggests that it is the difference between the mean transmission rates rather than the difference between the basic reproductive ratios, that determines such interference signature.

5. Discussion

For (one-host) two-disease systems, one of the fundamental questions concerns the coexistence of the two infections. By examining the existence and stability conditions of equilibria of the model, we have found that the conditions necessary for the two diseases to coexist are generally not particularly restrictive. This is partly because of the long host lifespan and the brief infectious period of the diseases, typical of most human diseases. Our results have demonstrated that the condition for competitive exclusion, may be significantly affected by the disease-induced mortality (ρ_is). Increases in these parameters result in a reduction of the coexistence region.
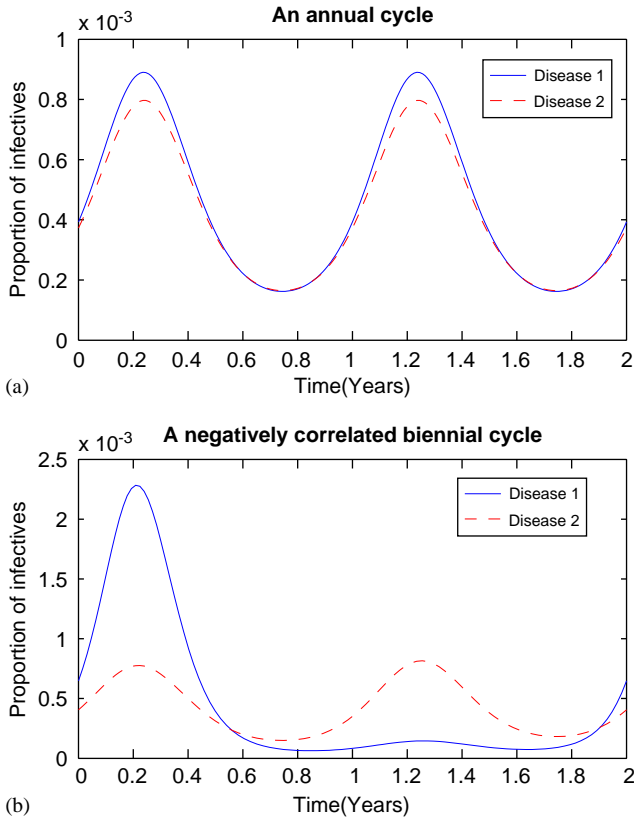
(a)

(b)

Fig. 9. A stable annual cycle ($\beta_{10} = 300$, $\gamma_1 = 40$) and a biennial cycle ($\beta_{10} = 400$, $\gamma_1 = 40$) for diseases 1 and 2 which exist in the corresponding regions in Fig. 8. Note that the two peaks of the biennial cycle for disease 2 do not differ greatly due to the mean transmission rate for disease 2 being small. Fixed parameters: $\beta_{20} = 250$, $\gamma_2 = 40$, $\sigma = 0.111$, $\delta_1 = \delta_2 = 35$, $\rho_1 = \rho_2 = 0$.

Using continuation methods, we have identified at least three types of attractor when the amplitude of seasonality is small: (i) annual cycles, (ii) biennial cycles in which the outbreaks of both infections are positively correlated, and (iii) negatively correlated biennial cycles. More complicated dynamics such as 4-year cycles and chaotic attractors are possible as the amplitude of seasonality is increased, but we have concentrated on parameters that we think realistic for childhood diseases (Keeling and Grenfell, 2002; Earn et al., 2000). It is interesting to note that the in-phase (or, negatively correlated) biennial dynamics (also reported in Rohani et al., 2003; Kamo and Sasaki, 2002) are highly sensitive to stochasticity. The introduction of noise (be it demographic or environmental) tends to force the outbreaks of the two infections out of phase. Understanding the precise mechanisms behind this finding is interesting and important, but is beyond the scope of the present study.

One of our main findings was that (for a fixed amplitude of seasonality) there is a threshold for the difference between mean transmission rates at which the

dynamical properties of the system bifurcated. It suggests that when the two-disease have similar mean transmission rates the system may exhibit complex dynamic interference patterns; in particular, multiple attractors, in which the two diseases are strongly correlated, can coexist.

Another interesting result is that in the presence of seasonality, the disease with the lower mean transmission rate mimics the dynamical behavior of the other infection. More precisely, when the mean transmission rate of one disease becomes sufficiently high the annual cycle of both diseases might undertake a period-doubling bifurcation, giving rise to biennial cycles which are not possible for the disease with a lower mean transmission rate when evaluated in a corresponding single-disease model. The result implies that one disease with a sufficiently higher mean transmission rate than the other, like the case of measles and whooping cough (Anderson and May, 1991; Rohani et al., 2002), may dominate the dynamical behavior of the system in which they interact.

The classic SIR (and SEIR) models have exposed some fundamental features of single-disease dynamics, such as the mechanisms that cause periodic dynamics and chaotic behaviors, with strong empirical evidence. The findings in this paper imply that for infections with a substantial convalescence period or an increased disease-induced mortality following infection, it may be impossible to understand epidemics by focusing on single-infection dynamics. Previous work (Rohani et al., 1998, 2003) has demonstrated that patterns from measles and whooping cough case fatality data in Europe are consistent with the predictions of two-disease models. Further analysis of these data are currently under way.

It has been argued by Rohani et al. (2003) that interference effects are most pronounced between infections with a similar basic reproductive ratio. The rationale behind this argument was that interference is most likely when diseases affect largely the same age-cohort, as dictated by the distribution of the age at infection. The next step in understanding disease interference is, therefore, to consider age-specific contact rates (Castillo-Chavez et al., 1989; Hethcote, 1988, 1997; Greenhalgh, 1988; Greenhalgh and Dietz, 1994; Diek-mann and Heesterbeek, 2000). We are currently exploring this issue.

Finally, we note that much of the approaches to studying immunological interactions between different strains of the same disease (as mediated by cross-immunity) can be "borrowed" to studying ecological interactions between different diseases (arising from convalescence or fatality). The former has been intensively studied, giving rise to a series of heuristic methods, concepts and theories (Castillo-Chavez et al., 1989; Andreasen et al., 1997; Kamo and Sasaki,

2002). A comprehensive comparison between the two topics would be an interesting issue that deserves attention.

Acknowledgments

Appendix A. Calculation of equilibria

An equilibrium is the solution of the following system of equations:

$$0 = -\beta_1(y_1 + z_1)x - \beta_2(y_2 + z_2)x - \mu x + \mu, \quad \text{(A.1)}$$
$$0 = \beta_1(y_1 + z_1)x - (\gamma_1 + \mu)y_1, \quad \text{(A.2)}$$
$$0 = \beta_2(y_2 + z_2)x - (\gamma_2 + \mu)y_2, \quad \text{(A.3)}$$
$$0 = \gamma_1 y_1 - (\delta_1 + \rho_1\delta_1 + \mu)u_1, \quad \text{(A.4)}$$
$$0 = \gamma_2 y_2 - (\delta_2 + \rho_2\delta_2 + \mu)u_2, \quad \text{(A.5)}$$
$$0 = \delta_2 u_2 - \beta_1(y_1 + z_1)v_1 - \mu v_1, \quad \text{(A.6)}$$
$$0 = \delta_1 u_1 - \beta_2(y_2 + z_2)v_2 - \mu v_2, \quad \text{(A.7)}$$
$$0 = \beta_1(y_1 + z_1)v_1 - (\gamma_1 + \mu)z_1, \quad \text{(A.8)}$$
$$0 = \beta_2(y_2 + z_2)v_2 - (\gamma_2 + \mu)z_2. \quad \text{(A.9)}$$

(i) For $y_1 = y_2 = 0$ we immediately obtain the disease-free equilibrium

$$E_1 = (1, 0, 0, 0, 0, 0, 0, 0, 0, 0). \quad \text{(A.10)}$$

(ii) For $y_1 \neq 0, y_2 = 0$ one finds that $u_2 = v_1 = z_1 = z_2 = 0$ while the rest of the equilibrium components are the solution of the following equations (with some new notations R_i, q_i which have been defined in the main text)

$$0 = -(\beta_1 y_1 + \mu)x + \mu, \quad \text{(A.11)}$$
$$0 = (R_1 x - 1)y_1, \quad \text{(A.12)}$$
$$0 = q_1 y_1 - u_1, \quad \text{(A.13)}$$
$$0 = \delta_1 u_1 - \mu v_2, \quad \text{(A.14)}$$

which yields an equilibrium $E_2 = (x^*, y_1^*, 0, u_1^*, 0, 0, v_2^*, 0, 0)$ in which

$$x^* = \frac{1}{R_1}, \quad y_1^* = \frac{\mu(R_1 - 1)}{\beta_1},$$
$$u_1^* = q_1 y_1^*, \quad v_2^* = \frac{\delta_1}{\mu}u_1^*. \quad \text{(A.15)}$$

One can easily derive the other single-disease endemic equilibrium E_3 by symmetry. Note that the secondary parameters R_i, q_i and a_i have been defined in (2.20)–(2.22), respectively.

(iii) For $y_1 \neq 0, y_2 \neq 0$, we find, by, respectively, summing up (A.2) and (A.8) and (A.3) and (A.9), that

$$v_i = \frac{1}{R_i} - x, \quad i = 1, 2 \quad \text{(A.16)}$$

while (A.4) and (A.5) gives

$$u_i = q_i y_i = q_i R_i(y_i + z_i), \quad i = 1, 2, \quad \text{(A.17)}$$

where we used the relation $y_i = R_i(y_i + z_i)$ given by (A.2) and (A.3). Substituting these relations into (A.6) and (A.7) one finds that

$$\delta_2 q_2 R_2(y_2 + z_2)x$$
$$= (\beta_1(y_1 + z_1) + \mu)\left(\frac{1}{R_1} - x\right), \quad \text{(A.18)}$$

$$\delta_1 q_1 R_1(y_1 + z_1)x$$
$$= (\beta_2(y_2 + z_2) + \mu)\left(\frac{1}{R_2} - x\right), \quad \text{(A.19)}$$

where

$$x = \frac{\mu}{\beta_1(y_1 + z_1) + \beta_2(y_2 + z_2) + \mu} \quad \text{(A.20)}$$

as a result of Eq. (A.1).
By denoting

$$W_i \equiv \beta_i(y_i + z_i), \quad i = 1, 2, \quad \text{(A.21)}$$

we end up with two decoupled equations

$$(W_1 + \mu)(W_1 + W_2 + \mu)$$
$$= \mu R_1(W_1 + a_2 W_2 + \mu), \quad \text{(A.22)}$$
$$(W_2 + \mu)(W_1 + W_2 + \mu)$$
$$= \mu R_2(a_1 W_1 + W_2 + \mu). \quad \text{(A.23)}$$

The two equations (A.22) and (A.23) define two hyperbolas in (W_1, W_2) plane

$$W_j = \frac{(W_i + \mu)[(W_i + \mu) - \mu R_i]}{-(W_i + \mu) + \mu R_i a_j}, \quad \text{(A.24)}$$

which have exactly one intersecting point in the positive quadrant if and only if

$$R_1 > 1, \quad R_2 > 1 \quad \text{(A.25)}$$

and

$$R_1 > \frac{R_2}{1 + a_2(R_2 - 1)} \quad \text{and}$$
$$R_2 > \frac{R_1}{1 + a_1(R_1 - 1)}. \quad \text{(A.26)}$$

This intersecting point corresponds to a positive equilibrium which we denote as E_4.

Appendix B. Linear stability analysis of E_2

Let us rearrange the components of the state variable as $(x, y_1, y_2, z_1, z_2, u_1, u_2, v_1, v_2)$. The Jacobian of the linearized system evaluated at an equilibrium $(x^*, y_1^*, y_2^*, z_1^*, z_2^*, u_1^*, u_2^*, v_1^*, v_2^*)$ has the following form:

$$
B = \begin{pmatrix}
b_{11} & -\beta_1 x^* & -\beta_2 x^* & -\beta_1 x^* & -\beta_2 x^* & 0 & 0 & 0 & 0 \\
w_1^* & b_{22} & 0 & \beta_1 x^* & 0 & 0 & 0 & 0 & 0 \\
w_2^* & 0 & b_{33} & 0 & \beta_2 x^* & 0 & 0 & 0 & 0 \\
0 & \beta_1 v_1^* & 0 & b_{44} & 0 & 0 & 0 & w_1^* & 0 \\
0 & 0 & \beta_2 v_2^* & 0 & b_{55} & 0 & 0 & 0 & w_2^* \\
0 & \gamma_1 & 0 & 0 & 0 & b_{66} & 0 & 0 & 0 \\
0 & 0 & \gamma_2 & 0 & 0 & 0 & b_{77} & 0 & 0 \\
0 & -\beta_1 v_1^* & 0 & -\beta_1 v_1^* & 0 & 0 & \delta_2 & b_{88} & 0 \\
0 & 0 & -\beta_2 v_2^* & 0 & -\beta_2 v_2^* & \delta_1 & 0 & 0 & b_{99}
\end{pmatrix},
$$

where $b_{11} = -(w_1^* + w_2^* + \mu)$, $b_{22} = \beta_1 x^* - (\gamma_1 + \mu)$, $b_{33} = \beta_2 x^* - (\gamma_2 + \mu)$, $b_{44} = \beta_1 v_1^* - (\gamma_1 + \mu)$, $b_{55} = \beta_2 v_2^* - (\gamma_2 + \mu)$, $b_{66} = -(\delta_1 + \mu)$, $b_{77} = -(\delta_2 + \mu)$, $b_{88} = -(W_1^* + \mu)$ and $b_{99} = -(W_2^* + \mu)$ while $w_i^* = \beta_i(y_i^* + z_i^*)$ (for $i = 1, 2$). For equilibrium E_2, we have $y_2^* = z_2^* = u_2^* = v_1^* = 0$ while the non-zero components x^*, y_1^*, u_1^* and v_2^* are given by (A.15). The corresponding characteristic polynomial can be computed as

$$
\begin{aligned}
|\lambda I_9 - J| = {} & [\lambda + (y_1^* + \mu)][\lambda + \mu][\lambda + (\delta_1 + \mu)] \\
& \times [\lambda + (\delta_2 + \mu)][\lambda + (\gamma_1 + \mu)] \\
& \times [\lambda^2 + (\beta_1 y_1^* + \mu)\lambda + \beta_1^2 x^* y_1^*] \\
& \times \Big[\lambda^2 - \frac{\beta_2}{R_2}(R_2(x^* + v_2^*) - 2)\lambda \\
& \quad - \frac{\beta_2^2}{R_2^2}(R_2(x^* + v_2^*) - 1)\Big].
\end{aligned}
\tag{B.27}
$$

It is easy to see that all roots other than those of the last quadratic factor are negative. The last quadratic factor can be further elaborated as

$$
\begin{aligned}
& \lambda^2 - \frac{\beta_2}{R_2}\left(R_2 \frac{1 + a_1(R_1 - 1)}{R_1} - 2\right)\lambda \\
& \quad - \frac{\beta_2^2}{R_2^2}\left(R_2 \frac{1 + a_1(R_1 - 1)}{R_1} - 1\right)
\end{aligned}
\tag{B.28}
$$

whose two roots are

$$
\lambda_1 = \frac{\beta_2}{R_2}\left(\frac{R_2(1 + a_1(R_1 - 1))}{R_1} - 1\right), \quad \lambda_2 = -\frac{\beta_2}{R_2},
$$

which are both negative if $R_1/(1 + a_1(R_1 - 1)) > R_2$. The equilibrium E_2 thus is stable as long as this condition is met. Note that the stability of E_2 also requires $R_1 > 1$ which guarantees the existence of E_2. Since the Jacobian matrix B has no purely imaginary eigenvalues at any circumstances, there is no Hopf bifurcation associated with E_2.

References

Anderson, R.M., May, R.M., 1991. Infectious Diseases of Humans. Oxford University Press, Oxford.

Andreasen, V.J., Lin, J., Levin, S.A., 1997. The dynamics of co-circulating influenza strains conferring partial cross-immunity. J. Math. Biol. 35, 825–842.

Aron, J.L., Schwartz, I.B., 1984. Seasonality and period-doubling bifurcations in an epidemic model. J. Theor. Biol. 110, 665–679.

Bartlett, M.S., 1956. Deterministic and stochastic models for recurrent epidemics. In: Neyman, J. (Ed.), Proceedings of the Third Berkeley Symposium on Mathematical Statistics and Probability, Berkeley. University of California Press, California, pp. 81–109.

Bauch, C.T., Earn, D.J.D., 2003. Transients and attractors in epidemics. Proc. R. Soc. London B 270, 1573–1578.

Bolker, B.M., Grenfell, B.T., 1993. Chaos and biological complexity in measles dynamics. Proc. R. Soc. London B 251, 75–81.

Bolker, B.M., Grenfell, B.T., 1995. Space, persistence and dynamics of measles. Philos. Trans. R. Soc. London B 348, 309–320.

Castillo-Chavez, C., Hethcote, H.W., Andreasen, V., Levin, S.A., Liu, W.M., 1989. Epidemiological models with age structure, proportionate mixing, and cross-immunity. J. Math. Biol. 27, 233–258.

Diekmann, O., Heesterbeek, J.A.P., 2000. Mathematical Epidemiology of Infectious Diseases: Model Building, Analysis and Interpretation. Wiley, New York.

Dietz, K., 1976. The incidence of infectious diseases under the influence of seasonal fluctuation. Lect. Notes Biomath. 11, 1–5.

Dietz, K., 1979. Epidemiological interference of virus populations. J. Math. Biol. 8, 291–300.

Doedel, E.J., Champneys, A.R., Fairgrieve, T.F., Kuznetsov, Yu.A., Wang, X., 1998. AUTO 97: CONTINUATION AND BIFURCATION SOFTWARE FOR ORDINARY DIFFERENTIAL EQUATIONS (with HomCont). Concordia University, Montreal, Canada.

Earn, D.J.D., Rohani, P., Bolker, B.M., Grenfell, B.T., 2000. A simple model for dynamical transitions in epidemics. Science 287, 667–670.

Gog, J.R., Swinton, J.A., 2002. A status-based approach to multiple strain dynamics. J. Math. Biol. 44, 169–184.

Greenhalgh, D., 1988. Threshold and stability results for an epidemic models with an age-structured meeting rate. IMA J. Math. Appl. Med. Biol. 5, 81–100.

Greenhalgh, D., Dietz, K., 1994. Some bounds on estimates for reproductive ratios derived from age-specific force of infection. Math. Biosci. 124, 9–57.

Gumel, A.B., Moghadas, S.M., Yuan, Y., Yu, P., 2003. Bifurcation and stability analysis of a 13-d SEIC model using normal form reduction and numerical analysis. Dynamics Continuous Discrete Impulsive Systems Ser. B: Appl. Algorithms 10, 317–330.

Gupta, S., Trenholme, K., Anderson, R.M., Day, K., 1994. Antigenic diversity and the transmission dynamics of *Plasmodium falciparum*. Science 263, 961–963.

Hethcote, H.W., 1988. Optimal age of vaccination for measles. Math. Biosci. 89, 28–52.

Hethcote, H.W., 1997. An age-structured model for pertussis transmission. Math. Biosci. 145, 89–136.

Kamo, M., Sasaki, A., 2002. The effect of cross-immunity and seasonal forcing in a multi-strain epidemic model. Physics D 165, 228–241.

Keeling, M.J., Grenfell, B.T., 2002. Understanding the persistence of measles: reconciling theory, simulation and observation. Proc. R. Soc. London B 269, 335–343.

Kirschner, D., 1999. Dynamics of co-infection with Tuberculosis and HIV-1. Theor. Popul. Biol. 55, 94–109.

Kuznetsov, Yu.A., 1998. Elements of Applied Bifurcation Theory. Springer, Berlin.

Kuznetsov, Yu.A., Piccardi, C., 1994. Bifurcation analysis of periodic *SEIR* and *SIR* epidemic models. J. Math. Biol. 32, 109–121.

Nowak, M.A., May, R.M., 1994. Super-infection and the evolution of virulence. Proc. R. Soc. London B 255, 81–89.

Rohani, P., Earn, D.J., Finkenstadt, B., Grenfell, B.T., 1998. Population dynamic interference among childhood diseases. Proc. R. Soc. London B 265, 2033–2041.

Rohani, P., Earn, D.J.D., Grenfell, B.T., 1999. Opposite patterns of synchrony in sympatric disease metapopulations. Science 286, 968–971.

Rohani, P., Keeling, M.J., Grenfell, B.T., 2002. The interplay between noise and determinism in childhood diseases. Am. Nat. 159, 469–481.

Rohani, P., Green, G.J., Mantilla-Beniers, N.B., Grenfell, B.T., 2003. Ecological interference between fatal diseases. Nature 422, 885–888.

Schenzle, D., 1984. A age-structured model of pre- and post-vaccination measles transmission. IMA. J. Math. Appl. Med. Biol. 1, 169–191.

Smith, H.L., 1983a. Subharmonic bifurcation in an SIR epidemic model. J. Math. Biol. 17, 163–177.

Smith, H.L., 1983b. Multiple stable subharmonics for a periodic epidemic model. J. Math. Biol. 17, 179–190.

Tompkins, D.M., Greenman, J.V., Hudson, P.J., 2001. Differential impact of shared nematode parasite on two gamebird hosts: implications for apparent competition. Parasitology 122, 187–193.